Minimizing Voltage Loss in Wide-Bandgap Perovskites for Tandem Solar Cells

Jaysankar, Manoj; Raul, Benedito A. L.; Bastos, Joao; Burgess, Claire; Weijtens, Christ; Creatore, Mariadriana; Aernouts, Tom; Kuang, Yinghuan; Gehlhaar, Robert; Hadipour, Afshin

Published in:
ACS Energy Letters

DOI:
10.1021/acsenergylett.8b02179

Publication date:
2019

ACS Energy LETTERS

Cite This: ACS Energy Lett. 2019, 4, 259−264

http://pubs.acs.org/journal/aelccp

LETTER

Minimizing Voltage Loss in Wide-Bandgap Perovskites for Tandem Solar Cells

Manoj Jaysankar,*[,†,‡] Benedito A. L. Raul,[§] Joao Bastos,[†,‡] Claire Burgess,[∥] Christ Weijtens,[∥] Mariadriana Creatore,[∥] Tom Aernouts,[†] Yinghuan Kuang,[†] Robert Gehlhaar,[†] Afshin Hadipour,[†] and Jef Poortmans[†,‡]

[†]Imec − Partner in Solliance, Kapeldreef 75, 3000 Leuven, Belgium

[‡]Department of Electrical Engineering, KU Leuven, 3000 Leuven, Belgium

[§]Zernike Institute for Advanced Materials, University of Groningen, 9712 CP Groningen, Netherlands

[∥]Department of Applied Physics, TU Eindhoven, 5600 MB Eindhoven, Netherlands

Supporting Information

ABSTRACT: **Perovskites with bandgaps between 1.7 and 1.8 eV are optimal for tandem configurations with crystalline silicon (c-Si) because they facilitate efficient harvest of solar energy. In that respect, achieving a high open-circuit voltage (V_{OC}) in such wide-bandgap perovskite solar cells is crucial for a high overall power conversion efficiency (PCE). Here, we provide key insights into the factors affecting the V_{OC} in wide-bandgap perovskite solar cells. We show that the influence of the hole transport layer (HTL) on V_{OC} is not simply through its ionization potential but mainly through the quality of the perovskite−HTL interface. With effective interface passivation, we demonstrate perovskite solar cells with a bandgap of 1.72 eV that exhibit a V_{OC} of 1.22 V. Furthermore, by combining the high-V_{OC} perovskite solar cell with a c-Si solar cell, we demonstrate a perovskite−Si four-terminal tandem solar cell with a PCE of 27.1%, exceeding the record PCE of single-junction Si solar cells.**

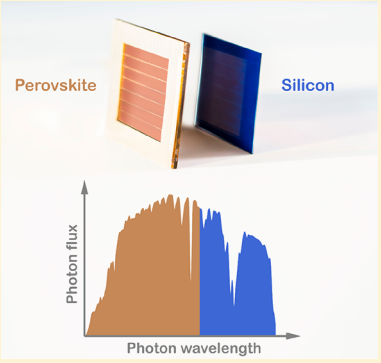

In recent years, hybrid organometallic halide perovskite solar cells have proven to be promising candidates for low-cost, wide-bandgap top solar cells in tandem configuration with market-leading crystalline silicon (c-Si) solar cells.[1−6] Perovskite−Si tandem solar cells hold the potential of surpassing the theoretical power conversion efficiency (PCE) limits of established photovoltaic technologies.[6−10] The promise of high PCE is made possible by the remarkable electronic properties of the perovskite absorber.[11,12] One such property that is of particular interest for tandem applications is seamless tunability of the perovskite bandgap (E_G) by varying the stoichiometry of the perovskite absorber.[13−15] Bandgap tuning in the widely used methylammonium lead halide perovskite is usually achieved by partially substituting the iodide halide for bromide, with higher bromide content leading to a wider bandgap. In this fashion, the bandgap of methylammonium halide perovskite can be tuned from the most common 1.56 eV up to 2.3 eV.[14,16]

The possibility of optimizing the bandgap of the top solar cell based on the bottom solar cell facilitates achieving maximal tandem PCE by minimizing thermalization losses. In order to achieve maximal tandem PCE with a perovskite−Si tandem solar cell, a perovskite with a bandgap of 1.7−1.8 eV (wide-bandgap) is deemed optimal.[7,17] Solar cells employing such wide-bandgap perovskites, hereon referred to as wide-bandgap perovskite solar cells, are also expected to exhibit higher open-circuit voltages (V_{OC}) than the solar cells using the more common 1.5−1.6 eV perovskites. However, such wide-bandgap mixed-halide perovskite solar cells currently suffer from V_{OC} deficits (defined as $E_G/q - V_{OC}$) larger than 0.65 V that limit their performance.[14,15,18−20] Such a large V_{OC} deficit exhibited by wide-bandgap mixed-halide perovskite solar cells has previously been attributed to several causes, including light-induced phase segregation and energy levels of hole transport layers (HTLs).[16,21−23]

In this work, we investigate key factors limiting the V_{OC} of wide-bandgap mixed-halide perovskite solar cells. First, we demonstrate photostable wide-bandgap mixed-halide perovskite solar cells with a bandgap of 1.72 eV. Second, we show that key to achieving high V_{OC} is careful control of the perovskite−HTL interface. Through effective interface passivation, we fabricate 1.72 eV mixed-halide perovskite solar cells with a V_{OC} deficit as low as 0.5 V. By combining the high V_{OC} wide-bandgap perovskite solar cell with a c-Si solar cell, we demonstrate four-terminal perovskite−Si tandem solar cells exhibiting a PCE of

Received: November 12, 2018
Accepted: December 12, 2018
Published: December 12, 2018

DOI: 10.1021/acsenergylett.8b02179
ACS Energy Lett. 2019, 4, 259−264

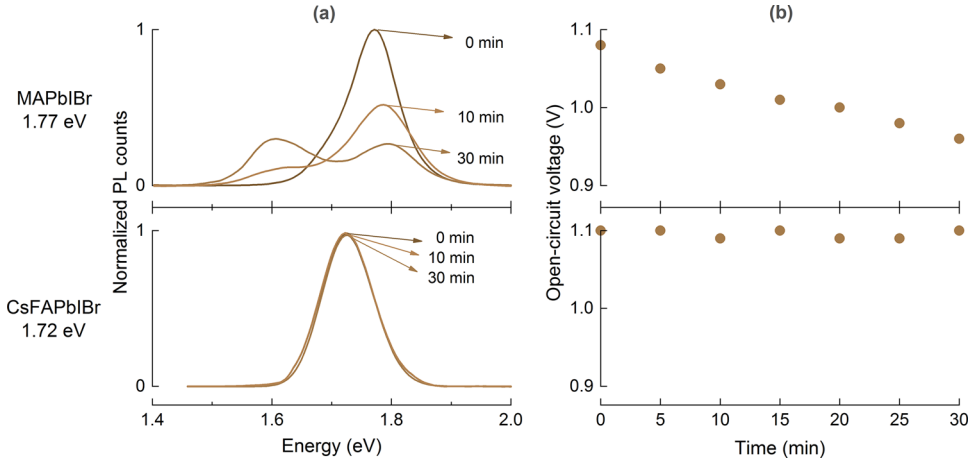

Figure 1. (a) PL spectra of MAPbIBr and CsFAPbIBr thin films under continuous AM 1.5G irradiation. (b) Evolution of the open-circuit voltage of MAPbIBr and CsFAPbIBr solar cells under continuous illumination.

27.1%, the highest reported for a perovskite-based four-terminal solar cell.

The architecture of the perovskite solar cells investigated in this work is as follows: glass/ITO/SnO_2/perovskite/HTL/ITO/MgF_2 (Figure S1). The photostability of two different mixed-halide perovskites, namely, methylammonium lead iodide−bromide, $CH_3NH_3Pb(I_{0.6}Br_{0.4})_3$ (MAPbIBr) with a bandgap of 1.77 eV, and cesium formamidinium lead iodide−bromide, $Cs_{0.15}(CH_5N_2)_{0.85}Pb(I_{0.71}Br_{0.29})_3$ (CsFAPbIBr) with a bandgap of 1.72 eV, was investigated. Details about device fabrication are described in the Supporting Information. The phase stability of these perovskite thin films deposited on glass substrates and light-soaked under continuous AM 1.5G illumination was characterized by photoluminescence (PL) measurements. The PL response of MAPbIBr thin films changes over time, with the PL peak corresponding to the pristine MAPbIBr perovskite phase splitting into two separate peaks over time (Figure 1a). The splitting of the PL peak indicates segregation of the pristine MAPbIBr perovskite phase into iodide-rich and bromide-rich phases under illumination. The iodide-rich phase (indicated by the PL peak at 1.56 eV) limits the electrical performance, resulting in a V_{OC} reduction of the MAPbIBr solar cells over time (Figure 1b).[14] This observation is in line with previous reports of light-induced phase segregation in MAPbIBr perovskite thin films.[23]

On the other hand, the CsFAPbIBr perovskite thin films show similar PL response with no peak splitting even after 30 min of light-soaking (Figure 1a). The unchanging PL response of CsFAPbIBr thin films indicates better photostability of the CsFAPbIBr perovskite compared to the MAPbIBr perovskite. The results are consistent with theoretical findings which show that exchanging the MA cation for Cs and FA cations results in better photostability likely through a combination of favorable thermodynamics, crystallinity, and lower halide vacancy densities.[24,25] Additionally, long-term light stability tests reveal no undue degradation of the 1.72 eV mixed-halide CsFAPbIBr solar cells compared with standard 1.56 eV pure-iodide CsFAPbI perovskite solar cells, which have been shown to be photostable (Figure S2).[26] The photostability is also reflected in the stable V_{OC} of CsFAPbIBr solar cells over time (Figure 1b). Although these solar cells exhibit stable voltage output, their V_{OC} deficit is still 0.62 V. Such a large V_{OC} deficit is unfavorable for tandem applications considering the limited current density of wide-bandgap perovskite solar cells.

In addition to phase segregation, the effect of the HTL ionization potential on V_{OC} of the perovskite solar cells was investigated. Accordingly, CsFAPbIBr perovskite solar cells with different HTLs were fabricated and characterized. The layer stack of the solar cells is shown in Figure S1a. Figure 2 plots the

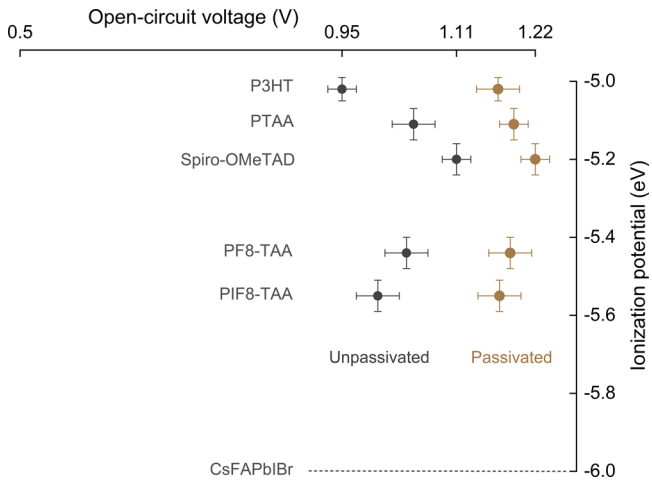

Figure 2. Open-circuit voltages of CsFAPbIBr solar cells with different HTLs with and without 0.8 nm of an ALD Al_2O_3 passivation layer. The measured ionization potential of CsFAPbIBr perovskite is shown for reference.

V_{OC} of CsFAPbIBr solar cells as a function of ionization potential of the different HTLs. The ionization potential of CsFAPbIBr perovskite measured with ultraviolet photoelectron spectroscopy (UPS) is also indicated for reference. The ionization potentials of the different HTLs were obtained from the literature.[16,27−32] The unpassivated CsFAPbIBr solar cells with different HTLs exhibit V_{OC} in the range of 0.95 to 1.11 V without clear correlation with the HTL ionization potential, similar to the observation of Belisle et al.[28] The lack of a conclusive trend suggests the V_{OC} of the perovskite solar cell may not be simply influenced by the ionization potential of the HTL as long as there is no barrier for hole extraction. Moreover, the champion cell still exhibits a considerable V_{OC} deficit of 0.62 V.

To further understand the cause of the high V_{OC} deficit, the evolution of V_{OC} with temperature was monitored. The V_{OC} of

DOI: 10.1021/acsenergylett.8b02179
ACS Energy Lett. 2019, 4, 259−264

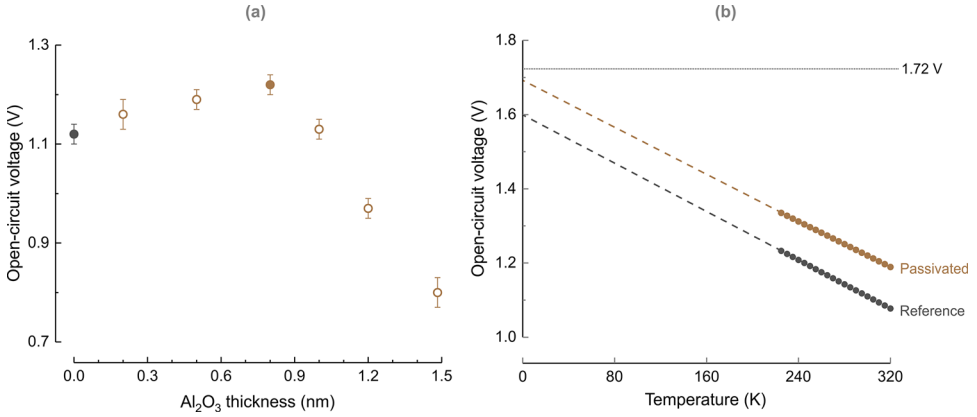

Figure 3. (a) Effect of interfacial Al_2O_3 layer thickness on the open-circuit voltage of CsFAPbIBr solar cells with spiro-OMeTAD as the HTL. (b) Evolution of the open-circuit voltage with temperature for CsFAPbIBr solar cells without Al_2O_3 (reference) and with an 0.8 nm interfacial Al_2O_3 layer (passivated). The dashed lines show linear extrapolation of measured values of the open-circuit voltage to absolute zero temperature. The horizontal dotted line indicates the bandgap of CsFAPbIBr divided by the elementary charge.

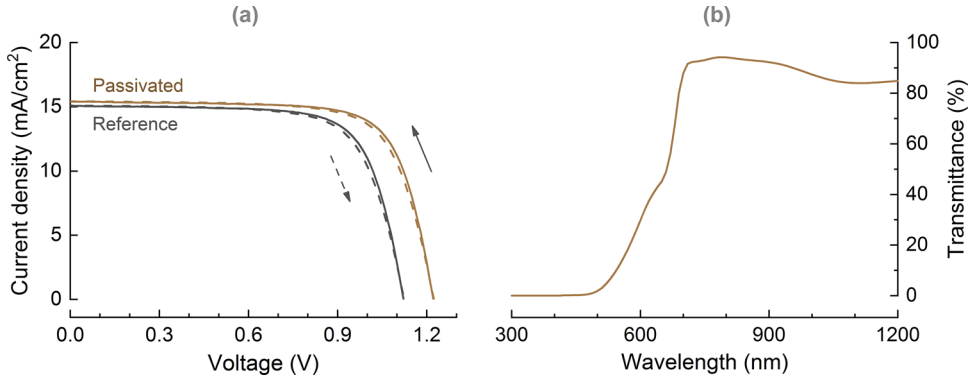

Figure 4. (a) Current density−voltage characteristics of semitransparent CsFAPbIBr solar cells without Al_2O_3 (reference) and with a 0.8 nm interfacial Al_2O_3 layer (passivated) measured in forward and reverse directions. (b) Transmittance spectra of a passivated semitransparent CsFAPbIBr solar cell.

the CsFAPbIBr solar cell increases linearly with decreasing temperature (Figure S3). By extrapolating the measured V_{OC} values to absolute zero temperature, the activation energy (E_A) of the dominant recombination mechanism is estimated using the following relation[33]

$$qV_{OC} = E_A - nk_BT \ln\left(\frac{J_{00}}{J_{ph}}\right)$$

where J_{00} is a prefactor of the reverse saturation current density J_0, J_{ph} is the photocurrent density, n is the ideality factor of the solar cell, k_B is the Boltzmann constant, q is the elementary charge, and T is the absolute temperature. A significant offset between E_A and the perovskite bandgap implies that V_{OC} of the solar cell is strongly influenced by nonradiative recombination at interfaces of the absorber in addition to the bulk.[33−35] In addition, the magnitude of the offset is inversely related to the quality of the interface. For the CsFAPbIBr solar cells investigated in this study, the E_A varies with the choice of HTL (Figure S3). The CsFAPbIBr solar cell with spiro-OMeTAD as the HTL (reference solar cell) has the highest E_A of 1.60 eV, which corresponds to an offset of 0.12 eV with the perovskite bandgap. The offset is smallest for the reference spiro-OMeTAD devices compared to devices with other HTLs denoting better interface quality of CsFAPbIBr with spiro-OMeTAD than that with the other HTLs. The better interface results in a higher V_{OC} of CsFAPbIBr solar cells with spiro-OMeTAD as the HTL (Figure 2). These measurements indicate that the CsFAPbIBr−HTL interface quality is a key factor influencing V_{OC} of the solar cells.

With a view to reduce the V_{OC} deficit and boost the V_{OC} of CsFAPbIBr solar cells, we focused on further improving the quality of the interface between CsFAPbIBr and spiro-OMeTAD. Inspired by the work of Koushik et al.[36] where a thin Al_2O_3 layer was used to improve the performance of methylammonium lead iodide solar cells, we introduce a layer of Al_2O_3 at the CsFAPbIBr−HTL interface by atomic layer deposition (ALD) (Figure S1b). Figure 3a shows the impact of Al_2O_3 thickness on V_{OC} of CsFAPbIBr solar cells. It should be noted that the Al_2O_3 thicknesses were extracted based on the number of ALD cycles and the growth rate on polished c-Si substrates. Although a difference in growth rate on different substrates can be encountered in ALD deposition, it is typically accepted that the key parameters for ultrathin layers are the number of ALD cycles and the corresponding growth rate on c-Si. In our case, an optimal Al_2O_3 thickness for improved V_{OC} is achieved for 45 ALD cycles (~0.8 nm). Beyond 45 cycles, the Al_2O_3 is presumably too thick, creating a barrier for hole extraction due to its dielectric characteristic. The optimally thick layer of Al_2O_3 yields a maximal gain of 110 mV in V_{OC} (Figure 3a). Introducing the ALD-grown Al_2O_3 improves V_{OC} likely through passivation of dangling bonds at the interface, thus

DOI: 10.1021/acsenergylett.8b02179
ACS Energy Lett. 2019, 4, 259−264

Table 1. Photovoltaic Parameters of Semitransparent CsFAPbIBr Perovskite and c-Si Solar Cells Measured under 1000 W m^{-2} AM 1.5G Irradiance[a]

device	aperture area (cm^2)	J_{SC} (mA/cm^2)	V_{OC} (V)	fill factor (%)	aperture PCE_{SPO} (%)
reference CsFAPbIBr	0.13	15.1 ± 0.13	1.11 ± 0.03	70.1 ± 0.7	11.7 ± 0.1
passivated CsFAPbIBr	0.13	15.4 ± 0.11	1.22 ± 0.02	73.4 ± 0.4	13.8 ± 0.1
	4	14.0 ± 0.14	8.51 ± 0. 19	70.9 ± 0.6	12.1 ± 0.1
c-Si stand-alone	4	41.3 ± 0.02	0.691 ± 0.002	80.6 ± 0.1	23.0 ± 0.01
c-Si in tandem	4	24.1 ± 0.03	0.678 ± 0.002	81.2 ± 0.1	13.3 ± 0.03
CsFAPbIBr–Si tandem	0.13				27.1 ± 0.1
	4				25.3 ± 0.1

[a]The reported power conversion efficiency, PCE_{SPO}, is the stabilized power output of the solar cells tracked at the maximum power point for 10 min.

reducing nonradiative recombination of charge carriers.[36,37] Introducing the ALD Al_2O_3 layer results in significant V_{OC} increase also in the cases where HTLs other than spiro-OMeTAD are used (Figure 2). Moreover, upon passivating the perovskite–HTL interface, the spread in V_{OC} is limited when varying HTLs. The passivated CsFAPbIBr solar cells with spiro-OMeTAD as the HTL exhibit the highest V_{OC} of 1.22 V with a V_{OC} deficit of just 0.5 V. The Al_2O_3 passivation also increases the E_A in the solar cell to 1.68 eV, reducing its offset with the bandgap to a negligible value of 0.04 eV (Figure 3b). The reduced offset implies improved interface quality and reduced impact of interfacial recombination on V_{OC}. Because the reduced offset is marginal, it also implies that V_{OC} of the passivated CsFAPbIBr solar cell is now limited by nonradiative recombination in the bulk of the perovskite. Further improvement in V_{OC} can be expected by improving the bulk quality of the perovskite layer through effective processing techniques that lead to fewer bulk defects.

The current–voltage characteristics of reference and passivated CsFAPbIBr solar cells are shown in Figure 4a. The Al_2O_3 passivation significantly improves the V_{OC} and fill factor of the solar cells, boosting the PCE from 11.7 to 13.8% in the case of 0.13 cm^2 cells (Figure 4a). Detailed photovoltaic parameters are tabulated in Table 1. Furthermore, the CsFAPbIBr solar cells exhibit an average transmittance of 90% in the wavelength range of 700–1200 nm (Figure 4b). The high transmittance coupled with high V_{OC} makes the passivated CsFAPbIBr solar cells attractive for highly efficient tandem solar cells. To that end, four-terminal tandem solar cells were fabricated by combining the passivated CsFAPbIBr solar cells with IBC c-Si solar cells. Their wider bandgap of CsFAPbIBr allows additional light to reach the bottom Si solar cell, enabling efficient harvesting of solar irradiation (Figures S4 and S6). The resulting CsFAPbIBr–Si tandem solar cells exhibit a PCE of 27.1% on 0.13 cm^2, the highest reported for a perovskite-based four-terminal tandem solar cell, exceeding the record PCE of single-junction Si solar cells (Table 1).[38] Furthermore, semitransparent mini-modules employing seven serially interconnected passivated CsFAPbIBr perovskite subcells with an overall aperture area of 4 cm^2 were fabricated by the procedure described in our earlier work.[4] The semitransparent CsFAPbIBr mini-modules were stacked on top of IBC c-Si solar cells in a module-on-cell architecture to realize 4 cm^2 tandem solar modules where the dimensions of top and bottom devices are identical. The module-on-cell tandem devices exhibit an overall PCE of 25.3% on a 4 cm^2 aperture area, significantly surpassing the stand-alone PCEs of the individual devices (Table 1).

In summary, the factors affecting V_{OC} in wide-bandgap mixed-halide perovskite solar cells were investigated. In solar cells with phase-stable wide-bandgap perovskite, the choice of HTL material has an impact on V_{OC} not simply due to its ionization potential but through the quality of the perovskite–HTL interface. Passivation of the perovskite–HTL interface by Al_2O_3 significantly enhances V_{OC}, reducing the V_{OC} deficit in wide-bandgap mixed-halide CsFAPbIBr solar cells to just 0.5 V. The high V_{OC} and transmittance of the passivated CsFAPbIBr solar cells enable 27.1% efficient four-terminal CsFAPbIBr–Si tandem solar cells, surpassing the current record of single-junction Si solar cells. Our results provide valuable insights into the V_{OC} deficit in perovskite solar cells and suggest a path toward high V_{OC} perovskite solar cells.

■ ASSOCIATED CONTENT

Supporting Information

The Supporting Information is available free of charge on the ACS Publications website at DOI: 10.1021/acsenergylett.8b02179.

Detailed device fabrication and characterization methods including additional plots (PDF)

■ AUTHOR INFORMATION

Corresponding Author

*E-mail: manoj.jaysankar@imec.be.

ORCID

Manoj Jaysankar: 0000-0002-2727-295X

Joao Bastos: 0000-0002-8877-9850

Notes

The authors declare no competing financial interest.

■ ACKNOWLEDGMENTS

This work has been supported by Solliance, a partnership of R&D organizations from The Netherlands, Belgium, and Germany working on thin-film photovoltaic solar energy. Additionally, the work was partially funded by the European Union's Horizon 2020 research and innovation program under Grant Agreement No. 764047 (ESPResSo). M.C. and C.B. are grateful for financial support from the Dutch Ministry of Economic Affairs, via The Top-consortium Knowledge and Innovation (TKI) Program "High-Efficiency Si Perovskite Tandem Solar Cells (HIPER)" (TEUE116193).

■ REFERENCES

(1) Bush, K. A.; Palmstrom, A. F.; Yu, Z.; Boccard, M.; Cheacharoen, R.; Mailoa, J. P.; McMeekin, D. P.; Hoye, R. L. Z.; Bailie, C. D.; Leijtens, T.; et al. 23.6%-Efficient Monolithic Perovskite/Silicon Tandem Solar Cells with Improved Stability. *Nat. Energy* **2017**, *2* (4), 17009.

DOI: 10.1021/acsenergylett.8b02179
ACS Energy Lett. 2019, 4, 259–264

(2) Werner, J.; Barraud, L.; Walter, A.; Bräuninger, M.; Sahli, F.; Sacchetto, D.; Tétreault, N.; Paviet-Salomon, B.; Moon, S.-J.; Allebé, C.; et al. Efficient Near-Infrared-Transparent Perovskite Solar Cells Enabling Direct Comparison of 4-Terminal and Monolithic Perovskite/Silicon Tandem Cells. *ACS Energy Lett.* **2016**, *1* (2), 474−480.
(3) Sahli, F.; Werner, J.; Kamino, B. A.; Bräuninger, M.; Monnard, R.; Paviet-Salomon, B.; Barraud, L.; Ding, L.; Diaz Leon, J. J.; Sacchetto, D.; et al. Fully Textured Monolithic Perovskite/Silicon Tandem Solar Cells with 25.2% Power Conversion Efficiency. *Nat. Mater.* **2018**, *17* (9), 820−826.
(4) Jaysankar, M.; Qiu, W.; van Eerden, M.; Aernouts, T.; Gehlhaar, R.; Debucquoy, M.; Paetzold, U. W.; Poortmans, J. Four-Terminal Perovskite/Silicon Multijunction Solar Modules. *Adv. Energy Mater.* **2017**, *7* (15), 1602807.
(5) Duong, T.; Wu, Y.; Shen, H.; Peng, J.; Fu, X.; Jacobs, D.; Wang, E.; Kho, T. C.; Fong, K. C.; Stocks, M.; et al. Rubidium Multication Perovskite with Optimized Bandgap for Perovskite-Silicon Tandem with over 26% Efficiency. *Adv. Energy Mater.* **2017**, *7* (14), 1700228.
(6) Bailie, C. D.; Christoforo, M. G.; Mailoa, J. P.; Bowring, A. R.; Unger, E. L.; Nguyen, W. H.; Burschka, J.; Pellet, N.; Lee, J. Z.; Grätzel, M.; et al. Semi-Transparent Perovskite Solar Cells for Tandems with Silicon and CIGS. *Energy Environ. Sci.* **2015**, *8* (3), 956−963.
(7) Almansouri, I.; Ho-Baillie, A.; Bremner, S. P.; Green, M. A. Supercharging Silicon Solar Cell Performance by Means of Multijunction Concept. *IEEE J. Photovoltaics* **2015**, *5* (3), 968−976.
(8) Lal, N. N.; Dkhissi, Y.; Li, W.; Hou, Q.; Cheng, Y.; Bach, U. Perovskite Tandem Solar Cells. *Adv. Energy Mater.* **2017**, *7* (18), 1602761.
(9) Löper, P.; Moon, S.-J.; Martín de Nicolas, S.; Niesen, B.; Ledinsky, M.; Nicolay, S.; Bailat, J.; Yum, J.-H.; De Wolf, S.; Ballif, C. Organic−inorganic Halide Perovskite/Crystalline Silicon Four-Terminal Tandem Solar Cells. *Phys. Chem. Chem. Phys.* **2015**, *17* (3), 1619−1629.
(10) Jaysankar, M.; Filipič, M.; Zielinski, B.; Schmager, R.; Song, W.; Qiu, W.; Paetzold, U. W.; Aernouts, T.; Debucquoy, M.; Gehlhaar, R.; et al. Perovskite−silicon Tandem Solar Modules with Optimised Light Harvesting. *Energy Environ. Sci.* **2018**, *11* (6), 1489−1498.
(11) De Wolf, S.; Holovsky, J.; Moon, S.-J.; Löper, P.; Niesen, B.; Ledinsky, M.; Haug, F.-J.; Yum, J.-H.; Ballif, C. Organometallic Halide Perovskites: Sharp Optical Absorption Edge and Its Relation to Photovoltaic Performance. *J. Phys. Chem. Lett.* **2014**, *5* (6), 1035−1039.
(12) Stranks, S. D.; Eperon, G. E.; Grancini, G.; Menelaou, C.; Alcocer, M. J. P.; Leijtens, T.; Herz, L. M.; Petrozza, A.; Snaith, H. J. Electron-Hole Diffusion Lengths Exceeding 1 Micrometer in an Organometal Trihalide Perovskite Absorber. *Science* **2013**, *342* (6156), 341−344.
(13) Jaysankar, M.; Qiu, W.; Bastos, J.; Tait, J. G.; Debucquoy, M.; Paetzold, U. W.; Cheyns, D.; Poortmans, J. Crystallisation Dynamics in Wide-Bandgap Perovskite Films. *J. Mater. Chem. A* **2016**, *4* (27), 10524−10531.
(14) Unger, E. L.; Kegelmann, L.; Suchan, K.; Sörell, D.; Korte, L.; Albrecht, S. Roadmap and Roadblocks for the Band Gap Tunability of Metal Halide Perovskites. *J. Mater. Chem. A* **2017**, *5* (23), 11401−11409.
(15) Rajagopal, A.; Yang, Z.; Jo, S. B.; Braly, I. L.; Liang, P.-W.; Hillhouse, H. W.; Jen, A. K. Y. Highly Efficient Perovskite-Perovskite Tandem Solar Cells Reaching 80% of the Theoretical Limit in Photovoltage. *Adv. Mater.* **2017**, *29* (34), 1702140.
(16) Ryu, S.; Noh, J. H.; Jeon, N. J.; Kim, Y. C.; Yang, W. S.; Seo, J.; Seok, S. Il. Voltage Output of Efficient Perovskite Solar Cells with High Open-Circuit Voltage and Fill Factor. *Energy Environ. Sci.* **2014**, *7*, 2614−2618.
(17) Lal, N. N.; White, T. P.; Catchpole, K. R. Optics and Light Trapping for Tandem Solar Cells on Silicon. *IEEE J. Photovoltaics* **2014**, *4* (6), 1380−1386.
(18) Noh, J. H.; Im, S. H.; Heo, J. H.; Mandal, T. N.; Seok, S. Il. Chemical Management for Colorful, Efficient, and Stable Inorganic-Organic Hybrid Nanostructured Solar Cells. *Nano Lett.* **2013**, *13* (4), 1764−1769.
(19) Rajagopal, A.; Stoddard, R. J.; Jo, S. B.; Hillhouse, H. W.; Jen, A. K.-Y. Overcoming the Photovoltage Plateau in Large Bandgap Perovskite Photovoltaics. *Nano Lett.* **2018**, *18* (6), 3985−3993.
(20) Eperon, G. E.; Hörantner, M. T.; Snaith, H. J. Metal Halide Perovskite Tandem and Multiple-Junction Photovoltaics. *Nat. Rev. Chem.* **2017**, *1* (12), 0095.
(21) Draguta, S.; Sharia, O.; Yoon, S. J.; Brennan, M. C.; Morozov, Y. V.; Manser, J. M.; Kamat, P. V.; Schneider, W. F.; Kuno, M. Rationalizing the Light-Induced Phase Separation of Mixed Halide Organic−inorganic Perovskites. *Nat. Commun.* **2017**, *8* (1), 200.
(22) Edri, E.; Kirmayer, S.; Cahen, D.; Hodes, G. High Open-Circuit Voltage Solar Cells Based on Organic-Inorganic Lead Bromide Perovskite. *J. Phys. Chem. Lett.* **2013**, *4* (6), 897−902.
(23) Hoke, E. T.; Slotcavage, D. J.; Dohner, E. R.; Bowring, A. R.; Karunadasa, H. I.; McGehee, M. D. Reversible Photo-Induced Trap Formation in Mixed-Halide Hybrid Perovskites for Photovoltaics. *Chem. Sci.* **2015**, *6* (1), 613−617.
(24) Slotcavage, D. J.; Karunadasa, H. I.; McGehee, M. D. Light-Induced Phase Segregation in Halide-Perovskite Absorbers. *ACS Energy Lett.* **2016**, *1* (6), 1199−1205.
(25) Brennan, M. C.; Draguta, S.; Kamat, P. V.; Kuno, M. Light-Induced Anion Phase Segregation in Mixed Halide Perovskites. *ACS Energy Lett.* **2018**, *3* (1), 204−213.
(26) Lee, J.-W.; Kim, D.-H.; Kim, H.-S.; Seo, S.-W.; Cho, S. M.; Park, N.-G. Formamidinium and Cesium Hybridization for Photo- and Moisture-Stable Perovskite Solar Cell. *Adv. Energy Mater.* **2015**, *5* (20), 1501310.
(27) Chueh, C.-C.; Li, C.-Z.; Jen, A. K.-Y. Recent Progress and Perspective in Solution-Processed Interfacial Materials for Efficient and Stable Polymer and Organometal Perovskite Solar Cells. *Energy Environ. Sci.* **2015**, *8* (4), 1160−1189.
(28) Belisle, R. A.; Jain, P.; Prasanna, R.; Leijtens, T.; McGehee, M. D. Minimal Effect of the Hole-Transport Material Ionization Potential on the Open-Circuit Voltage of Perovskite Solar Cells. *ACS Energy Lett.* **2016**, *1* (3), 556−560.
(29) Schulz, P.; Edri, E.; Kirmayer, S.; Hodes, G.; Cahen, D.; Kahn, A. Interface Energetics in Organo-Metal Halide Perovskite-Based Photovoltaic Cells. *Energy Environ. Sci.* **2014**, *7* (4), 1377.
(30) Zhang, W.; Wang, Y.; Li, X.; Song, C.; Wan, L.; Usman, K.; Fang, J. Recent Advance in Solution-Processed Organic Interlayers for High-Performance Planar Perovskite Solar Cells. *Adv. Sci.* **2018**, *5*, 1800159.
(31) Luo, S.; Daoud, W. a. Recent Progress in Organic−inorganic Halide Perovskite Solar Cells: Mechanisms and Material Design. *J. Mater. Chem. A* **2015**, *3*, 8992−9010.
(32) Westbrook, R. J. E.; Sanchez-Molina, D. I.; Manuel Marin-Beloqui, D. J.; Bronstein, D. H.; Haque, D. S. A. Effect of Interfacial Energetics on Charge Transfer from Lead Halide Perovskite to Organic Hole Conductors. *J. Phys. Chem. C* **2018**, *122* (2), 1326−1332.
(33) Hegedus, S. S.; Shafarman, W. N. Thin-Film Solar Cells: Device Measurements and Analysis. *Prog. Photovoltaics* **2004**, *12* (23), 155−176.
(34) Kirchartz, T.; Rau, U. What Makes a Good Solar Cell? *Adv. Energy Mater.* **2018**, *8*, 1703385.
(35) Tress, W.; Yavari, M.; Domanski, K.; Yadav, P.; Niesen, B.; Correa Baena, J. P.; Hagfeldt, A.; Graetzel, M. Interpretation and Evolution of Open-Circuit Voltage, Recombination, Ideality Factor and Subgap Defect States during Reversible Light-Soaking and Irreversible Degradation of Perovskite Solar Cells. *Energy Environ. Sci.* **2018**, *11* (1), 151−165.
(36) Koushik, D.; Verhees, W. J. H.; Kuang, Y.; Veenstra, S.; Zhang, D.; Verheijen, M. A.; Creatore, M.; Schropp, R. E. I. High-Efficiency Humidity-Stable Planar Perovskite Solar Cells Based on Atomic Layer Architecture. *Energy Environ. Sci.* **2017**, *10* (1), 91−100.
(37) Wang, J. T.-W.; Wang, Z.; Pathak, S.; Zhang, W.; deQuilettes, D. W.; Wisnivesky-Rocca-Rivarola, F.; Huang, J.; Nayak, P. K.; Patel, J. B.; Mohd Yusof, H. A.; et al. Efficient Perovskite Solar Cells by Metal Ion Doping. *Energy Environ. Sci.* **2016**, *9* (9), 2892−2901.

DOI: 10.1021/acsenergylett.8b02179
ACS Energy Lett. 2019, 4, 259−264

(38) Green, M. A.; Hishikawa, Y.; Dunlop, E. D.; Levi, D. H.; Hohl-Ebinger, J.; Ho-Baillie, A. W. Y. Solar Cell Efficiency Tables (Version 52). *Prog. Photovoltaics* **2018**, *26* (7), 427−436.

DOI: 10.1021/acsenergylett.8b02179
ACS Energy Lett. 2019, 4, 259−264